IOP Conf. Series: Materials Science and Engineering **278** (2017) 012165 doi:10.1088/1757-899X/278/1/012165

Periodic flow hydrodynamic resistance parameters for woven screen matrices at cryogenic temperatures

M D Perrella and S M Ghiaasiaan

G.W. Woodruff School of Mechanical Engineering, Georgia Institute of Technology, Atlanta, GA, 30332, USA

Abstract. The regenerator is a critical component in all Stirling and Pulse Tube cryocoolers. It generally consists of a microporous metallic or rare-earth filler material contained within a cylindrical shell. Accurate modelling of the hydrodynamic and thermal behaviour of different regenerator materials is crucial to the successful design of cryogenic systems. Previous investigations have used experimental measurements at steady and periodic flow conditions in conjunction with pore-level CFD analysis to determine the pertinent hydrodynamic parameters, namely the Darcy permeability and Forchheimer coefficients. Due to the difficulty associated with experimental measurement at cryogenic temperatures, past investigations were mostly performed at ambient conditions and their results are assumed to be appropriate for cryogenic temperatures. In this study, a regenerator filled with woven screen matrices such as 400 mesh T316 stainless steel were assembled and experimentally tested under periodic helium flow at cryogenic temperatures. The mass flow and pressure drop data were analysed using CFD to determine the dimensionless friction factor, Darcy Permeability and Forchheimer coefficients. These results are compared to previous investigations at ambient temperature conditions, and the relevance of room-temperature models and correlations to cryogenic temperatures is critically assessed.

1. Introduction

The regenerator is widely considered to be the most important component of any Stirling or Pulse Tube cryocooler. It typically consists of a thin-walled cylindrical shell packed with a porous filler material such as a particle bed, wire mesh, or metal foam. Because of the computational expense and other difficulties associated with the direct numerical simulation of fluid flow through the porous media, it is far more common to use a volume averaging approach to represent the overall impact of the filler material on the fluid [1–5]. When volume averaging is applied to the conservation of momentum equation, it yields the popular extended Darcy-Forchheimer model for flow through a porous medium which can be expressed as

$$\frac{\partial(\rho u)}{\partial t}+\frac{\partial}{\partial x}(\rho u^2)+\frac{\partial P}{\partial x}+\left(\frac{\varepsilon\mu}{K}u+\frac{c_f\varepsilon^2\rho}{\sqrt{K}}u^2\right)=0 \tag{1}$$

for transient, one-dimensional flow where K represents the Darcy permeability and c_f represents the Forchheimer inertial coefficient in the axial direction [6]. These parameters are frequently referred to as hydrodynamic resistance parameters and are used in commercially-available software to predict the performance of cryocooler regenerators and optimize the cooler's design. Such programs which are widely accepted and used in industry include Regen 3.3 from the National Institute of Science and Technology (NIST) [7] and Sage from Gedeon and Associates [8].

Content from this work may be used under the terms of the Creative Commons Attribution 3.0 licence. Any further distribution of this work must maintain attribution to the author(s) and the title of the work, journal citation and DOI.
Published under licence by IOP Publishing Ltd

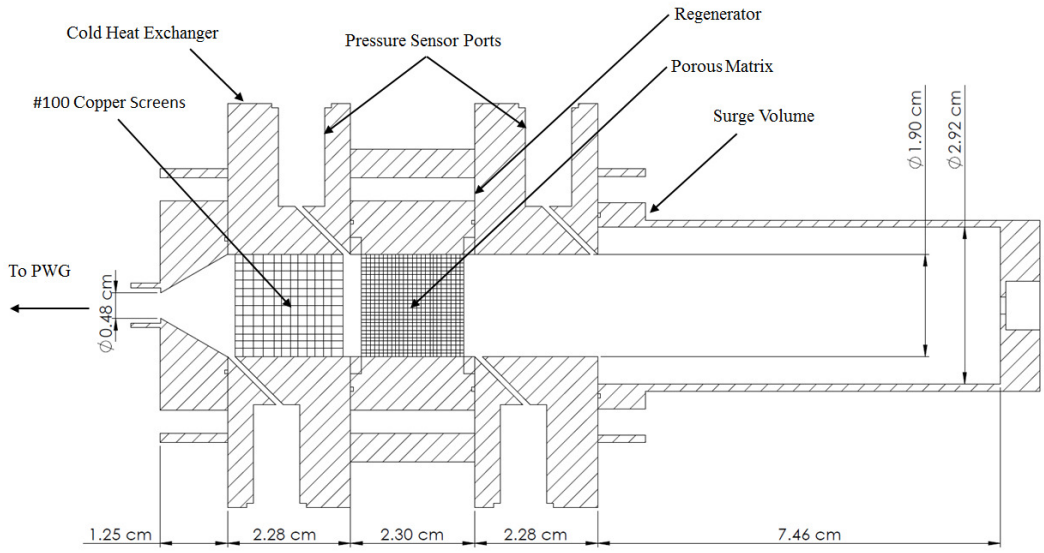

Figure 1. Schematic of experimental test section consisting of (from left to right) the Cold Heat Exchanger (CHX), prototypical regenerator filled with #400 SS mesh, and rigid surge volume.

There are two popular approaches for determining the hydrodynamic resistance parameters of various porous media: pore-level CFD modelling [9–11] and experimentation [12–17]. Experimentation is generally preferred due to the difficulties associated with precisely modelling the porous media on a microscopic level. However, due to the logistical difficulties associated with performing experimental measurements at cryogenic temperatures, each of these previous studies has been performed at room-temperature. In theory, the hydrodynamic resistance of the medium should not change with temperature so long as the microscopic pore structure remains the same. There is a pressing need in the literature, however, to verify the validity of the forgoing assumption to lend greater confidence to future cryocooler design and optimization.

2. Experimental Setup

2.1. Apparatus

The test section and its vicinity are shown schematically in figure 1. The test section consists of a stainless steel regenerator sandwiched between a heat exchanger and a rigid stainless steel surge volume (SV). An oscillatory flow of high-purity helium is induced by a Q-drive model 2S132W Pressure Wave Generator (PWG) upstream of the test section connected via a 0.91 m (3 ft) stainless steel transfer tube. A PowerFlex 700 power supply is used to specify the operating frequency and applied voltage of the PWG. The heat exchanger, or Cold Heat Exchanger (CHX), is thermally synched with the 1st stage of a Sumitomo model RDK-408D2 GM cryocooler by a copper bus bar. The interior of the CHX is packed with #100 mesh copper screens (porosity of 64.7%) to ensure adequate thermal contact and heat transfer with the helium working fluid. The regenerator is packed with #400 stainless steel screens with a porosity of 69.9% and wire diameter of 30.5 μm. The screens are retained by a rigid #60 stainless steel screen at the upstream and downstream locations. There are also 0.2 cm (0.07 in) deep void volumes created by retaining rings upstream and downstream of the regenerator, giving the porous matrix a total length of 1.9 cm. PCB piezotronics brand pressure sensors (models 102A05 and 102A10) are installed in specially designed ports on the upstream and downstream sides of the CHX and surge volume. The experimental setup and the GM cryocooler are mounted inside of a vacuum-sealed dewar with modular feedthroughs which is capable of maintaining an insulating vacuum of 10E-6 torr in order to reduce conduction and convection loads from the surroundings.

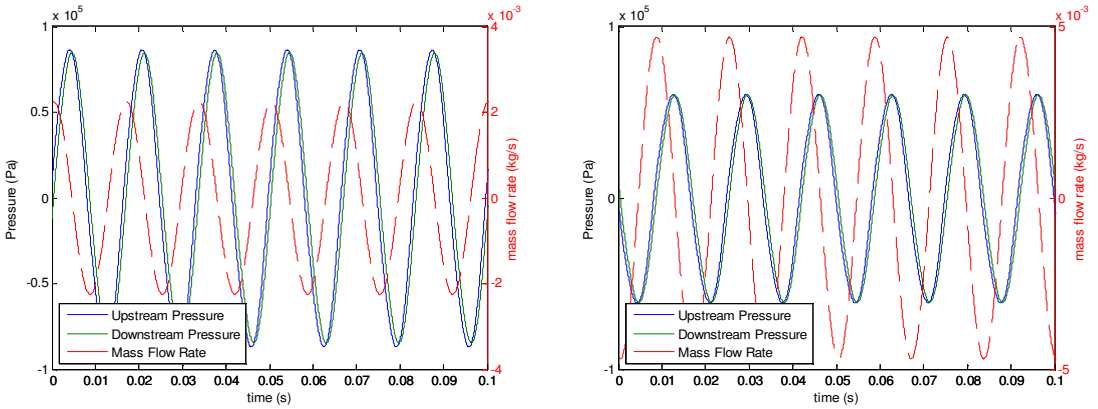

a) 60Hz 30V 2.86MPa 300K b) 60Hz 30V 2.86MPa 100K

Figure 2. Instantaneous pressure oscillations and mass flow rate through regenerator.

2.2. Data acquisition and analysis

Instantaneous pressure measurements were made upstream and downstream of the regenerator test section in 2-second durations at a sample rate of 25.6 Hz for a total of 51200 samples. A minimum of 6 individual 2-second measurements was taken at each PWG setting. The oscillatory pressure measurements were analyzed using Matlab's FFT capability. Analysis shows that the time-dependent pressure can be adequately expressed in terms of the pressure amplitude and phase using the first five fundamental frequencies as follows

$$P(t) = \sum_{i=1}^{i=5} P_i \cos(n\pi ft + \phi_i) \tag{2}$$

where n = 2, 4, 5, 8, 10. Temperatures are measured using a LakeShore Cryotronics Cernox temperature sensor mounted to the CHX. The mass flow exiting the regenerator test section is calculated indirectly by considering the instantaneous pressure and temperature within the SV.

$$\dot{m} = \frac{V}{\gamma RT}\frac{dP}{dt} \tag{3}$$

The time derivative of the SV pressure can be determined numerically from the collected data to calculate the instantaneous mass flow rate into the SV which can be expressed as a function of time where n = 2, 4, 5, 8, 10.

$$\dot{m}(t) = \sum_{i=1}^{i=5} \dot{m}_i \cos(n\pi ft + \phi_i) \tag{4}$$

2.3. Representative experimental results

Figure 2 shows typical oscillatory pressure measurements and mass flow rates for a mean operating pressure of 2.86 MPa at ambient and cryogenic temperatures. A pressure of zero on the y-axis refers to the mean operating pressure of the PWG. The difference between the mean operating pressures at different locations along the test section is assumed to be negligible compared to the effect of the pressure amplitude and phase shift on the mass flow. The maximum mass flow rate occurs when the difference between the upstream and downstream pressure across the regenerator is greatest. When the upstream and downstream pressures are equal, the mass flow rate is zero. The figure shows that for the same frequency and voltage input pressure amplitude decreases with decreasing temperature while mass flow rate increases due to the increased density of the gas. Pressure amplitude and mass flow rate amplitude also decrease with decreasing mean pressure. Figure 3 presents the maximum instantaneous pressure drop across the regenerator as a function of the peak experimental physical velocity through the regenerator for mean operating pressures of 2.86, 1.13, and 0.26 MPa and

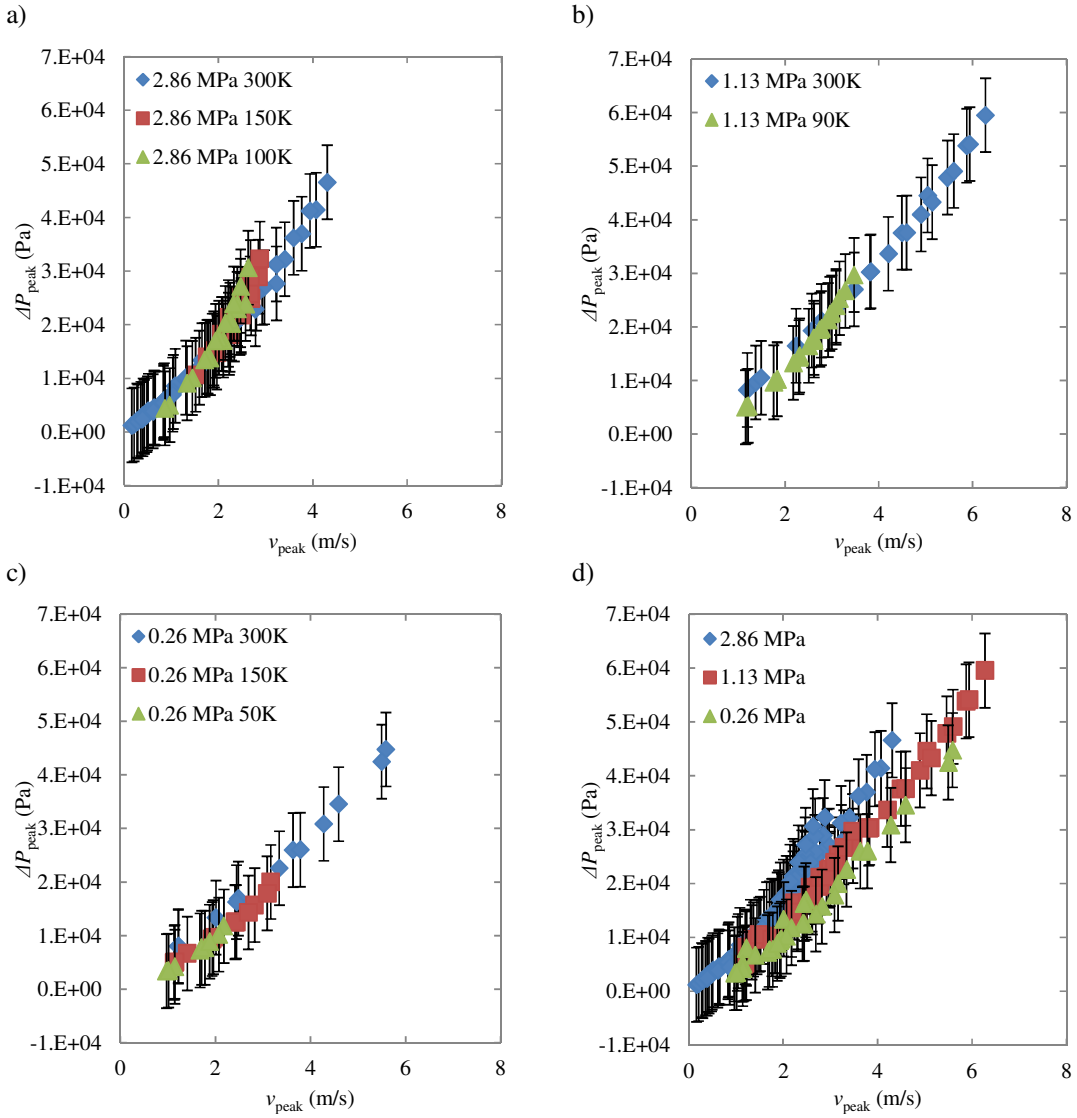

Figure 3. Maximum instantaneous pressure drop across regenerator as a function of peak physical flow velocity for mean pressures of (a) 2.86 MPa, (b) 1.13 MPa, and (c) 0.26 MPa at ambient and cryogenic temperatures. Figure (d) presents a combined view.

frequencies of 50, 60, and 70 Hz for ambient and cryogenic temperatures. The results indicate that the pressure drop across the regenerator is independent of frequency when plotted versus the flow velocity, therefore all frequencies are represented with the same markers. Per the manufacturer's specifications, the systematic uncertainty of the 102A05 and 102A10 pressure sensors is $\leq 1\%$ of the full scale value of 690 kPa, which gives a total uncertainty of 6.9 kPa. This is shown by the error bars in Figure 3.

3. Modelling methodology

To extract the hydrodynamic resistance parameters from the experimental data, a two-part computational approach is utilized. First Sage, a one-dimensional numerical software for cryocooler design and optimization, is used to create a computational model of the entire test section which is then optimized by varying the compressor stroke and regenerator friction factor, *f*, to match the experimental results. Second, ANSYS Fluent CFD software is used to simulate the regenerator and

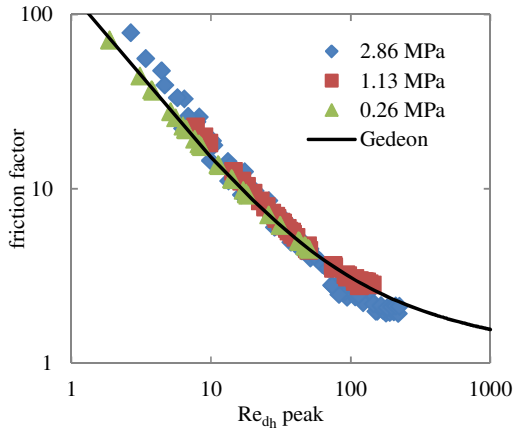

Figure 4. Sage friction factor using the generic matrix filler material to match experimental data versus the hydraulic diameter-based Reynolds number.

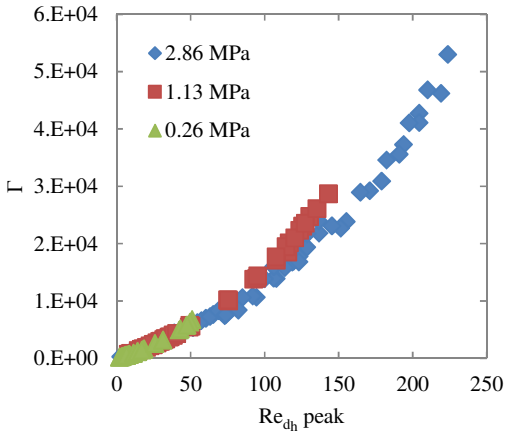

Figure 5. Non-dimentionalized porous media momentum source term, Γ, versus hydraulic diameter-based Reynolds number for 2.86, 1.13, and 0.26 MPa.

surge volume with a two-dimensional axisymmetric model. The Sage friction factor is correlated with respect to the flow velocity in order to extract the viscous resistance, β, and inertial resistance, C_2, in Fluent notation which are synonymous with the Darcy permeability and Forchheimer coefficient, respectively.

3.1. Sage modelling approach

Sage uses a one-dimensional numerical solution technique to solve the conservation of mass, momentum, and energy equations given by the following [8].

$$\frac{\partial \rho A_f}{\partial t} + \frac{\partial \rho u A_f}{\partial x} = 0 \tag{5}$$

$$\frac{\partial \rho u A_f}{\partial t} + \frac{\partial u \rho u A_f}{\partial x} + \frac{\partial P}{\partial x} A_f - F A_f = 0 \tag{6}$$

$$\frac{\partial \rho e A_f}{\partial t} + P \frac{\partial A_f}{\partial t} + \frac{\partial}{\partial x}\left(u \rho e A_f + u P A_f + q\right) - Q_w = 0 \tag{7}$$

In the conservation of momentum given by Eq. (6) A_f represents the flow area, u represents the physical velocity in the primary or axial direction, and F represents the total frictional pressure gradient. The total frictional pressure gradient can be expressed in terms of the Sage friction factor, f, and the local loss coefficient, K as follows

$$F = \frac{\Delta P}{L} = -\left(\frac{f}{d_h} + \frac{K}{L}\right)\frac{\rho u |u|}{2} \tag{8}$$

The pressure drop through a regenerator packed with wire screens can be predicted using the following correlation developed by Gedeon and included in the Sage software package [18].

$$f = \frac{129}{\mathrm{Re}_{d_h}} + \frac{2.91}{\mathrm{Re}_{d_h}^{0.103}} \tag{9}$$

where Re_{dh} is the hydraulic diameter-based Reynold's number. In order to match the experimental data to the Sage model and determine the hydrodynamic resistance the generic matrix option in Sage was used where the friction factor is defined according to the following

$$f = c_1 + c_2 \mathrm{Re}_{d_h}^{\ m} + \frac{c_3}{\mathrm{Re}_{d_h}} \tag{10}$$

where the coefficients c_1, c_2, c_3, and m are defined by the user. For each experimental data point the compressor stroke and the friction factor coefficient, c_3, were iteratively varied using Sage's built-in optimization feature until the pressure amplitudes upstream and downstream of the simulated regenerator matched the experimental measurements. Figure 4 shows the results of matching the friction factor of the generic matrix to the experimental measurements, and demonstrates excellent agreement between these results and those provided by Eq. (9) for the entire range of operating frequencies, mean pressures and temperatures. This supports the belief that correlations for hydrodynamic resistance parameters developed at ambient temperatures, such as those of Gedeon et al. [18], are indeed applicable at cryogenic temperatures. For low flow rates, $\mathrm{Re}_{d_h} \leq 100$, the friction factor decreases proportionally to the inverse of the Reynolds number similar to internal laminar flow. Viscous forces appear to dominate in this region. For higher flow rates, $\mathrm{Re}_{d_h}>100$, the friction factor begins to plateau as inertial forces begin to have a greater effect on the hydrodynamic resistance. This follows the trend represented by Eq. (9).

3.2. CFD modelling approach

One drawback of the Sage modelling approach is that it does not differentiate between the viscous and inertial components of the hydrodynamic resistance. It is often useful to define separate coefficients to these components such as in the Darcy-Forcheimer model represented by Eq. (1). In Fluent [19], for example, the hydrodynamic resistance is represented by a momentum source term defined as

$$S_i = -\left(\frac{\varepsilon \mu}{\alpha} u_i + \frac{\varepsilon^2 C_2}{2} \rho |u| u_i \right) \tag{11}$$

for simple homogeneous porous media. The first term on the right hand side represents the viscous resistance of the medium, while the second term on the right hand side represents the inertial resistance. The conservation of mass and momentum in Fluent for flow through a porous medium are given by Eq (12) and Eq (13) , respectively.

$$\frac{\partial (\varepsilon \rho)}{\partial t} + \nabla \bullet \left(\varepsilon \rho \vec{u} \right) = 0 \tag{12}$$

$$\frac{\partial \left(\varepsilon \rho \vec{u} \right)}{\partial t} + \nabla \bullet \left(\varepsilon \rho \vec{u} \vec{u} \right) = -\varepsilon \nabla P + \nabla \bullet (\varepsilon \bar{\bar{\tau}}) + \varepsilon \vec{B}_f - \left(\frac{\varepsilon^2 \mu}{\alpha} \vec{u} + \frac{\varepsilon^3 C_2}{2} \rho |\vec{u}| \vec{u} \right) \tag{13}$$

Comparing the axial component of Eq. (13) to Eq. (6) indicates that the total frictional pressure gradient in Sage is identical to the momentum source term in Fluent. To extract the viscous and inertial resistance coefficients from the singular Sage friction factor, one need only correlate the total friction pressure gradient with respect to the flow velocity and apply a quadratic fit to the data. In practice, however, the changes in fluid properties that accompany changes in temperature and pressure make it difficult to fit all of the experimental data to a single correlation. The momentum source term can therefore be non-dimensionalized using the Reynolds number and hydraulic diameter as follows.

$$S_i \frac{\rho d_h^3}{\mu^2} = \frac{\varepsilon d_h^2}{\alpha} \mathrm{Re}_{d_h} + \frac{\varepsilon^2 C_2 d_h}{2} \mathrm{Re}_{d_h}^2 \tag{14}$$

$$\Gamma = \mathrm{A}\, \mathrm{Re}_{d_h} + \mathrm{B}\, \mathrm{Re}_{d_h}^2 \tag{15}$$

Figure 5 shows the results of the non-dimensionalization for all charge pressures and temperatures. A polynomial fit is performed to determine the values of the coefficient from Eq (15). These coefficients and the corresponding values for α and C_2 are provided in table 1. The viscous and inertial resistances from Fluent can then be expressed as the popular Darcy Permeability and Forcheimmer coefficients from Eq. (1) as follows.

$$K = \alpha \tag{16}$$

$$c_f = \frac{C_2 \sqrt{K}}{2} \tag{17}$$

Table 1. Summary of Fluent viscous and inertial resistance as well as Darcy Permeability and Forcheimer coefficient.

Pressure [MPa]	A	B	α [m^2]	C_2 [1/m]	K [m^2]	c_f
2.86	0.75	49.63	7.06E-11	4.33E+04	7.06E-11	1.82E-01
1.13	1.01	49.64	7.05E-11	5.88E+04	7.05E-11	2.47E-01
0.26	1.41	55.26	6.34E-11	8.17E+04	6.34E-11	3.25E-01
Combined	0.61	81.78	4.28E-11	3.50E+04	4.28E-11	1.16E-01
Cha [13]	-	-	2.52E-11	1.20E+05	2.52E-11	3.01E-01
Experimental	0.84	98.59	3.55E-11	4.87E+04	3.55E-11	1.45E-01

A CFD model was created for the regenerator and surge volume domains in Fluent. Modelling the regenerator and surge volume together creates a closed system model and eliminates the need for an outlet boundary condition. A mesh size of 6.35e-4 m was chosen for all simulations based on a mesh convergence study. A user defined function, or UDF, was written to apply an oscillating pressure boundary condition to the inlet of the regenerator based on the first five harmonics of the experimental pressure measurement. The results of the simulations are summarized in table 2. Error is evaluated based on the maximum instantaneous pressure and mass flow rate at the exit of the regenerator.

Table 2. Summary of simulation results compared to experimental measurements for several pressures and temperatures.

Pressure [MPa]	Temperature [K]	$\dot{m}_{exp}$ [kg/s]	$\dot{m}_{sim}$ [kg/s]	Percent error	$P_{max_{exp}}$ [Pa]	$P_{max_{sim}}$ [Pa]	Percent error
2.86	300	2.25E-03	1.76E-03	2.20E-01	8.46E+04	8.62E+04	1.79E-02
2.86	150	3.47E-03	2.76E-03	2.06E-01	6.49E+04	6.49E+04	3.35E-04
2.86	100	4.70E-03	3.85E-03	1.80E-01	6.03E+04	6.04E+04	9.35E-04
1.13	300	1.25E-03	1.02E-03	1.83E-01	4.81E+04	5.31E+04	1.04E-01
1.13	90	2.61E-03	2.10E-03	1.96E-01	3.14E+04	3.26E+04	3.99E-02
0.26	300	4.60E-04	3.99E-04	1.33E-01	1.83E+04	2.74E+04	5.00E-01
0.26	151	6.21E-04	4.83E-04	2.22E-01	1.24E+04	1.59E+04	2.87E-01
0.26	62	1.02E-03	7.93E-04	2.25E-01	8.22E+03	1.03E+04	2.58E-01

4. Conclusion

The results of the Fluent simulations agree well with the experimental data at higher pressures but appear to diverge more significantly at lower mean pressures. The reason for this is currently unknown. It is possible that the assumption of uni-directional flow within the porous medium is less valid at low pressures than at high, but more work will be needed to determine this for certain. The experimental and simulation results both indicate that the hydrodynamic resistance parameters of the porous medium are indeed independent of temperature as previously suspected. This will lend greater confidence to existing correlations and aid in the study of new regenerator filler materials in the future.

5. References

[1] Ochoa-Tapia, J. A., and Whitaker, S., 1995, "Momentum transfer at the boundary between a porous medium and a homogeneous fluid—I. Theoretical development," Int. J. Heat Mass Transf., **38**(14), pp. 2635–2646.
[2] Ochoa-Tapia, J. A., and Whitaker, S., 1997, "Heat transfer at the boundary between a porous medium and a homogeneous fluid," Int. J. Heat Mass Transf., **40**(11), pp. 2691–2707.
[3] Ochoa-Tapia, J. A., and Whitaker, S., 1995, "Momentum transfer at the boundary between a porous medium and a homogeneous fluid—II. Comparison with experiment," Int. J. Heat Mass Transf., **38**(14), pp. 2647–2655.
[4] Whitaker, S., 1999, The method of Volume Averaging. Theory and Applications of Transport in Porous Media, Kluwer Academic Publishers.
[5] Whitaker, S., 1996, "The Forchheimer equation: A theoretical development," Transp. Porous Media, **25**(1), pp. 27–61.
[6] Harvey, J. P., 2003, "Oscillatory Compressible Flow and Heat Transfer in Porous Media – Application To Cryocooler Regenerators," (December).
[7] Gary, J., Gallagher, A. O., Radebaugh, R., Huang, Y., and Marquardt, E., 2008, "REGEN3 . 3 : USER MANUAL," (April).
[8] Gedeon, D., 2016, "Sage User 's Guide."
[9] Kim, S.-M., and Ghiaasiaan, S. M., 2009, "Numerical Modeling of Laminar Pulsating Flow in Porous Media," J. Fluids Eng., **131**(4), p. 41203.
[10] Pathak, M. G., and Ghiaasiaan, S. M., 2011, "Convective heat transfer and thermal dispersion during laminar pulsating flow in porous media," Int. J. Therm. Sci., **50**(4), pp. 440–448.
[11] Pathak, M. G., Mulcahey, T. I., and Ghiaasiaan, S. M., 2013, "Conjugate heat transfer during oscillatory laminar flow in porous media," Int. J. Heat Mass Transf., **66**, pp. 23–30.
[12] Cha, J. S., Ghiaasiaan, S. M., and Kirkconnell, C. S., 2008, "Oscillatory flow in microporous media applied in pulse - tube and Stirling - cycle cryocooler regenerators," Exp. Therm. Fluid Sci., **32**(6), pp. 1264–1278.
[13] Cha, J. J., 2007, "Hydrodynamic Parameters of Micro Porous Media for Steady and Oscillatory Flow: Application to Cryocooler Regenerators," (August).
[14] Clearman, W. M., Cha, J. S., Ghiaasiaan, S. M., and Kirkconnell, C. S., 2008, "Anisotropic steady-flow hydrodynamic parameters of microporous media applied to pulse tube and Stirling cryocooler regenerators," Cryogenics (Guildf)., **48**(3–4), pp. 112–121.
[15] Landrum, E. C., Conrad, T. J., Ghiaasiaan, S. M., and Kirkconnell, C. S., 2010, "Hydrodynamic parameters of mesh fillers relevant to miniature regenerative cryocoolers," Cryogenics (Guildf)., **50**(6–7), pp. 373–380.
[16] Landrum, E. C., Conrad, T. J., Ghiaasiaan, S. M., and Kirkconnell, C. S., 2008, "Effect of Pressure on Hydrodynamic Parameters of Several PTR Regenerator Fillers in Axial Steady Flow," Wire, **15**, pp. 335–342.
[17] Pathak, M. G., Patel, V. C., Ghiaasiaan, S. M., Mulcahey, T. I., Helvensteijn, B. P., Kashani, a., and Feller, J. R., 2013, "Hydrodynamic parameters for ErPr cryocooler regenerator fillers under steady and periodic flow conditions," Cryogenics (Guildf)., **58**, pp. 68–77.
[18] Gedeon, D., and Wood, J. G., 1996, "Oscillating-Flow Regenerator Test Rig: Hardware and Theory With Derived Correlations for Screens and Felts," NASA-Lewis Contract. Rep. 198422, (February).
[19] Fluent, 2011, "ANSYS FLUENT User â€™ s Guide," **15317**(November), p. 2498.